Strain distribution in $Zr_{64.13}Cu_{15.75}Ni_{10.12}Al_{10}$ bulk metallic glass investigated by *in situ* tensile tests under synchrotron radiation

M. Stoica,[1,a] J. Das,[1] J. Bednarcik,[2] H. Franz,[2] N. Mattern,[1] W. H. Wang,[3] and J. Eckert[1,4]
[1]*IFW Dresden, Institute for Complex Materials, P.O. Box 270116, D-01171 Dresden, Germany*
[2]*HASYLAB at Deutsches Elektronen-Synchrotron (DESY), Notkestr. 85, D-22607 Hamburg, Germany*
[3]*Institute of Physics, Chinese Academy of Sciences, Beijing 100080, China*
[4]*Institute of Materials Science, TU Dresden, D-01062 Dresden, Germany*

(Received 18 February 2008; accepted 30 April 2008; published online 10 July 2008)

We report on the evolution of the atomic-scale strain tensor of ductile $Zr_{64.13}Cu_{15.75}Ni_{10.12}Al_{10}$ bulk metallic glass under tensile loading by using x-ray synchrotron radiation. The same kind of samples was previously investigated under compressive loading and revealed yielding at 1690 MPa together with large deformability of up to 160% strain. In tension the samples fracture at a lower stress, 1500 MPa, with no sign of yielding or plastic deformation. With no macroplasticity observed under tension, large differences in the elastic constants obtained from the strain tensor and from ultrasonic sound velocity measurements are revealed. This paper presents in detail the measuring procedure as well as the calculation of the tensile tensor and pair distribution functions of $Zr_{64.13}Cu_{15.75}Ni_{10.12}Al_{10}$ at different stages of deformation. The results are discussed in comparison with other reported data obtained from x-ray diffraction measurements using synchrotron radiation. © *2008 American Institute of Physics*. [DOI: 10.1063/1.2952034]

I. INTRODUCTION

Bulk metallic glasses (BMGs) have many potential applications due to their unique properties as, for example, superior strength and high hardness, excellent corrosion resistance, and high wear resistance.[1,2] The high strength of BMGs is often accompanied by more or less pronounced plastic deformation and their deformation and fracture mechanisms are quite different from crystalline materials.[3–12] At temperatures below or around the glass transition and rather high strain rates metallic glasses deform by the formation of localized shear bands,[3–5,8] whereas homogeneous flow of the supercooled liquid is observed at elevated temperatures and/or low strain rates.[13,14] For the former case, it was previously considered that the compressive fracture usually proceeds along a shear plane inclined by 45° to the loading axis,[15] i.e., the maximum shear stress plane. However, several recent systematic investigations on glasses in different alloy systems indicate that the shear fracture always deviates from the maximum shear stress plane either under compression or under tension.[16–19]

High strength has been a long-standing objective pursued in metals and alloys. BMGs have strengths approaching the theoretical limit,[20] but their plasticity at room temperature is typically very low. In uniaxial tension, the plastic strain is almost zero.[21] For the majority of the known BMGs, the plastic strain at room temperature is very limited ($<2\%$) even under compression, resulting from pronounced shear localization and work softening. The lack of plasticity makes BMGs prone to catastrophic failure in load-bearing conditions and restricts their application. This also hinders the precise study of some fundamental issues in glasses, such as the deformation mechanism and the dynamics of plastic deformation, in which large plasticity is needed for detailed analysis.[21] Plastic deformation of metallic glasses at room temperature occurs through the formation and evolution of shear bands and is localized in thin shear bands.[22] Therefore, brittleness is regarded as an intrinsic defect of metallic glasses. Efforts have been made to enhance the plasticity of BMGs, mostly focusing on the fabrication of BMG composites.[23–27] Very recently, Liu *et al.*[28] succeeded to prepare several Zr-based BMGs which show an exceptional deformability and a high strain as revealed by compression tests. The samples which were able to endure maximum deformation (yielding at 1690 MPa, maximum true strain of 160%) had a composition of $Zr_{64.13}Cu_{15.75}Ni_{10.12}Al_{10}$. In order to correlate the extraordinary plasticity of the glasses with their structure, transmission electron microscopy (TEM) investigations were performed to reveal their microstructural features. It was found that the BMGs are composed of isolated dark zones, ranging from 2 to 5 μm in size, surrounded by continuous bright zones of about 0.5–1 μm in width.[28] The volume fraction of the bright zones was estimated to be $\sim 10\%$. The selected-area electron diffraction patterns of both bright and dark zones showed only broad rings, confirming the glassy nature of both zones. The detailed structure of the bright and dark zones was also examined by means of high resolution TEM and a mazelike pattern without any crystalline fringes was observed. The structural studies confirmed the chemical and compositional homogeneities and the single glassy nature of the BMGs (i.e., no indications for phase separation were found). It was supposed[28] that the very high deformability of these BMGs stems from this particular kind of structure, in which hard regions (the black zones) are surrounded by soft regions (the bright zones).

Several properties of amorphous materials including fa-

[a]Author to whom correspondence should be addressed. Tel.: +49 351 4659 644. FAX: +49 351 4659 452. Electronic mail: m.stoica@ifw-dresden.de.

tigue, fracture, and component performance are governed by the magnitude of strain fields around inhomogeneities such as local compositional variations, crystalline inclusions, voids, or cracks.[29] In the past years[29] a universal diffraction method for characterizing bulk stress and strain fields in amorphous materials was established. This method, employing synchrotron radiation, was successfully applied in order to reveal the effect of hydrostatic stress state on the atomic-scale structural changes in glasses at high pressure,[30] the change in free volume during annealing,[31] the strain in the crystalline phase in glass-matrix composites,[32,33] as well as for calculating the strain tensor in monolithic BMG below the elastic limit[29] or beyond the Hookean limit.[34] All the mentioned studies were done with the BMGs subjected to a compressive stress. Only very recently,[35] this investigation method was applied to evaluate the elastic behavior of two brittle BMGs [$Zr_{62}Al_8Ni_{13}Cu_{17}$ and $La_{62}Al_{14}(Cu_{5/6}Ag_{1/6})_{14}Co_5Ni_5$] subjected to tensile loading.

In this work, we performed strain scanning by x-ray diffraction (XRD) for the $Zr_{64.13}Cu_{15.75}Ni_{10.12}Al_{10}$ BMG. The diffraction images were recorded for samples under applied tensile loads and were stopped just before fracture. Even though this glass showed a remarkable deformability and enhanced compressive strain,[28] it does not show any plastic deformation upon tensile loading. Hence, the studies were done only in the elastic regime.

II. EXPERIMENTAL DETAILS

A. Sample preparation and experimental setup

BMG plates of 10 mm width, 1.25 or 1.75 mm thickness, and 50 mm length with composition $Zr_{64.13}Cu_{15.75}Ni_{10.12}Al_{10}$ were prepared by arc-melting and suction casting.[28] In order to obtain dog-bone shape specimens with $10\times2\times1$ mm^3 measurement section for the tensile tests, the as-cast plates were machined by spark erosion method to obtain the desired geometry. The surfaces of the specimens were carefully polished in order to reduce the surface roughness. The specimens were strained under tension (Kammrath and Weiss GmbH straining system with a maximum load of 5 kN) at room temperature *in situ* in the x-ray beam at HASYLAB at DESY (Hamburg, Germany) on the wiggler beamline BW5 at the DORIS positron storage ring using monochromatic synchrotron radiation ($\lambda=0.0119441$ nm) of 103.8 keV. The tensile load was increased in steps of 400 N. For each load, seven independent points (with 1 mm steps along the gauge length) in the middle part of the specimen were sequentially scanned. Due to the small scattering angles, the polarization correction is almost negligible.[36] The diffraction experiments were carried out in the Debye–Scherrer geometry. The layout of the experimental setup is shown in Fig. 1. The measured samples were exposed for 10 s to the well collimated incident beam having a cross section of 1×1 mm^2. Two-dimensional (2D) (2300×2300 pixels, 150×150 μm^2 pixel size) XRD patterns were collected using a MAR 345 2D image plate detector carefully mounted orthogonal to the x-ray beam. In order to cover the high-Q range ($Q=4\pi\sin(\theta)/\lambda$) up to 16.5 Å^{-1}, the distance between the 2D detector and the sample was adjusted to 50 cm. The diffraction pattern from LaB_6 was used to calibrate the sample-to-detector distance D and tilting of the image plate detector with respect to the beam axis.

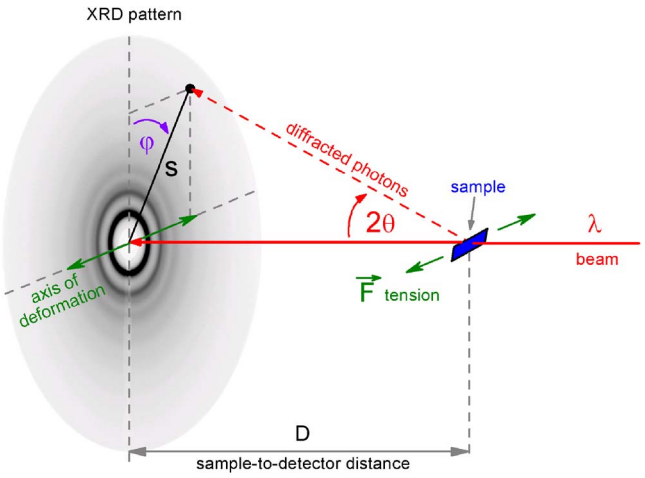

FIG. 1. (Color online) Sketch of an *in situ* tensile experiment. 2D diffraction pattern of $Zr_{64.13}Cu_{15.75}Ni_{10.12}Al_{10}$ metallic glass.

B. Determination of strain

The strain determination of bulk metallic glasses from XRD data is based on concepts previously reported by Poulsen *et al.*[29] Figure 2 shows an example for the raw data obtained for the $Zr_{64.13}Cu_{15.75}Ni_{10.12}Al_{10}$ glass without applied load. The symmetric circular diffraction pattern is characterized with respect to the polar coordinates (s,φ). By dividing the φ range of 0 to 2π into 36 segments, one obtains symmetrized intensity distributions

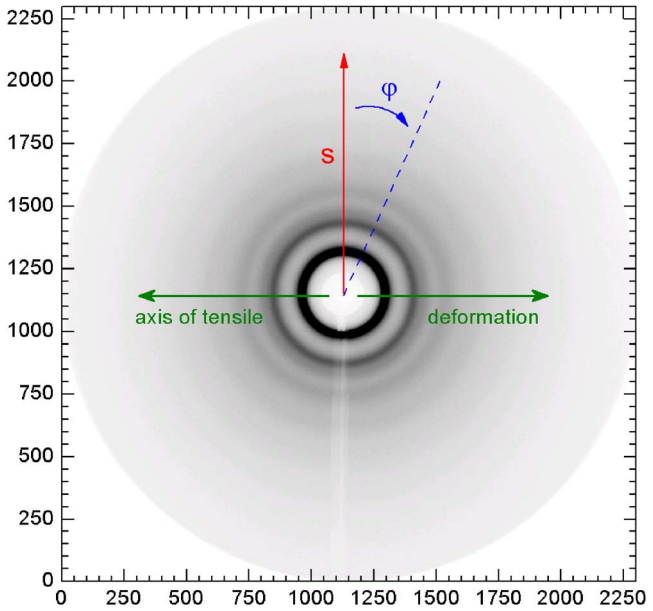

FIG. 2. (Color online) 2D diffraction pattern of $Zr_{64.13}Cu_{15.75}Ni_{10.12}Al_{10}$ metallic glass. The polar coordinates (s,φ) and the axis of deformation are depicted.

$$I_i'(Q,\varphi_i) = \int_{\varphi-\pi/36}^{\varphi+\pi/36} [I(Q,\varphi) + I(Q,\varphi+\pi)]d\varphi, \quad (1)$$

with $i=1\ldots18$, where $Q=Q(s)$ is defined by

$$Q(s) = \frac{4\pi}{\lambda}\sin\left[\frac{1}{2}\arctan\left(\frac{s}{D}\right)\right] \quad (2)$$

in which λ denotes the wavelength, D refers to the sample-to-detector distance, and s represents the distance from the origin of the polar coordinate system (see Fig. 1). Symmetrized intensity distributions as described by Eq. (1) were calculated using the software package FIT2D.[37] The procedure was repeated for all diffraction patterns acquired at different loads thus yielding the set of symmetrized distributions $I_i'(Q,\varphi,\sigma)$ where σ refers to the corresponding stress. For each $I_i'(Q,\varphi,\sigma)$ the shift in position of the first peak, $q(\varphi,\sigma)$, was determined with respect to the unloaded situation, $q(\varphi,0)$. The relative change in the position of the first peak upon applying an external stress defines the strain

$$\varepsilon_i(\varphi_i,\sigma) = \frac{q(\varphi_i,0) - q(\varphi_i,\sigma)}{q(\varphi_i,\sigma)}, \quad (3)$$

(with $i=1\ldots18$), which is angular dependent. The angular variation of the strain can be fitted to the following expression:

$$\varepsilon_\varphi(\varphi,\sigma) = \varepsilon_{11}\sin^2\varphi + \gamma_{12}\sin\varphi\cos\varphi + \varepsilon_{22}\cos^2\varphi. \quad (4)$$

As a result, the strain tensor can be determined, and the axial (ε_{11}), tangential (ε_{22}), and in-plane shear component (γ_{12}) can be derived. Components not in the plane perpendicular to the incoming beam can be determined by rotating the specimen around an axis perpendicular to the incoming beam. However, in the case of amorphous alloys this is not necessary since their structure is highly isotropic.

C. Determination of structure factor and pair distribution function

The data were then converted to the total structural function, $S(Q)$, using standard procedures described by Egami and Billinge.[38] The background intensity was subtracted directly from the diffraction pattern, and the 2D intensity distribution was integrated azimuthally with respect to the Q-space using the FIT2D (Ref. 37) software. The integrated data were corrected by considering polarization, sample absorption, fluorescence contribution, and inelastic scattering using the PDFGETX2 software.[39] The total structural factor $S(Q)$ is obtained from the normalized elastically scattered intensity, $I_e(Q)$

$$S(Q) = 1 + \frac{I_e(Q) - \left[\sum_{i=1}^{n} c_i f_i^2(Q)\right]}{\left[\sum_{i=1}^{n} c_i f_i^2(Q)\right]^2}, \quad (5)$$

where c_i and $f_i(Q)$ are the atomic concentration and the scattering factor of the atomic species of type i ($i=$Zr, Cu, Ni, Al), respectively. The corresponding reduced pair distribution function, $G(r)$, can be obtained through a sine Fourier transformation:

$$G(r) = 4\pi r[\rho(r) - \rho_0] = \frac{2}{\pi}\int_0^{Q_{\max}} Q(S(Q)-1)\sin(rQ)dQ, \quad (6)$$

where $\rho(r)$ and ρ_0 are the *local* and *average* atomic number densities, respectively, and r is the radial distance. From $G(r)$ the pair distribution function (PDF), $g(r)$, and the radial distribution function, RDF(r), can be calculated by

$$g(r) = \frac{\rho(r)}{\rho_0} = \frac{G(r)}{4\pi\rho_0 r} + 1, \quad (7)$$

$$\mathrm{RDF}(r) = 4\pi r^2\rho(r) = 4\pi r^2\rho_0 + rG(r). \quad (8)$$

The average coordination number, N, around any given atom in a spherical shell between radius r_1 and r_2 can be calculated as

$$N = \int_{r_1}^{r_2} \mathrm{RDF}(r)dr. \quad (9)$$

In order to resolve the nearest-neighbor partials from the first PDF peak, $G(r)$ is converted to $T(r)$ [$=4\pi r\rho(r)=4\pi r\rho_0(r)+G(r)$], in which the atomic pair distributions follow Gaussian profiles for isotropic systems such as amorphous alloys.[40] Thus, using a Gaussian to represent a partial [$4\pi r\rho_{ij}(r)$, where $\rho_{ij}(r)$ is the partial pair density function] one can express $T(r)$ as a sum of the weighted Gaussians

$$T(r) = \sum_i \sum_{j\le i} 4\pi r\rho_{ij}(r)w_{ij} = \sum_i \sum_{j\le i} w_{ij}\frac{a_{ij}}{\sqrt{2\pi\sigma_{ij}}}\exp\left[-\frac{(r-r_{ij})^2}{2\sigma_{ij}^2}\right], \quad (10)$$

where i and j denote the ith and jth atomic species, r_{ij} is the bond length of the i-j pair at the peak position, a_{ij} and σ_{ij} are the area and standard deviation of the Gaussian, and w_{ij} is the weight of the i-j pair, calculated in the following manner:

$$w_{ij} = \begin{cases} \dfrac{2c_ic_jf_i(0)f_j(0)}{\left[\sum_{k=1}^{n} c_kf_k(0)\right]^2}, & i \neq j \\ \dfrac{c_i^2f_i^2(0)}{\left[\sum_{k=1}^{n} c_kf_k(0)\right]^2}, & i = j \end{cases}. \quad (11)$$

III. RESULTS

A. Strain analysis

The 2D diffraction pattern of as-cast $Zr_{64.13}Cu_{15.75}Ni_{10.12}Al_{10}$ exhibits the diffuse scattering pattern typical for metallic glasses and confirms the presence of glassy structure without any hint for crystalline inclusions (see Fig. 2). The symmetric circular diffraction pattern is characteristic for the samples prior to applying tensile stress.

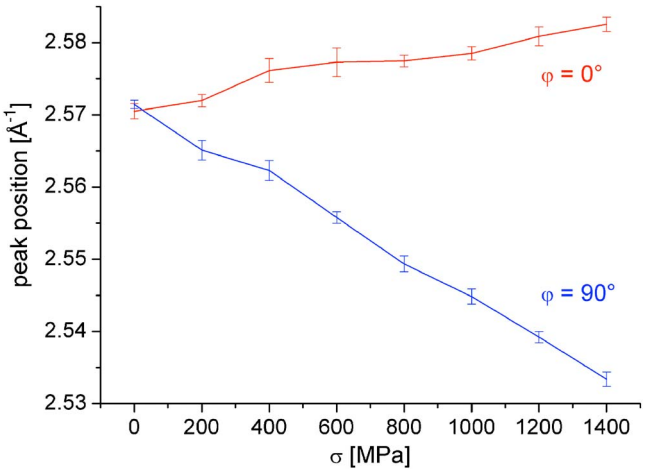

FIG. 3. (Color online) Change in the first peak position with applied tensile stress observed in tensile (φ=90°) and transversal (φ=0°) direction.

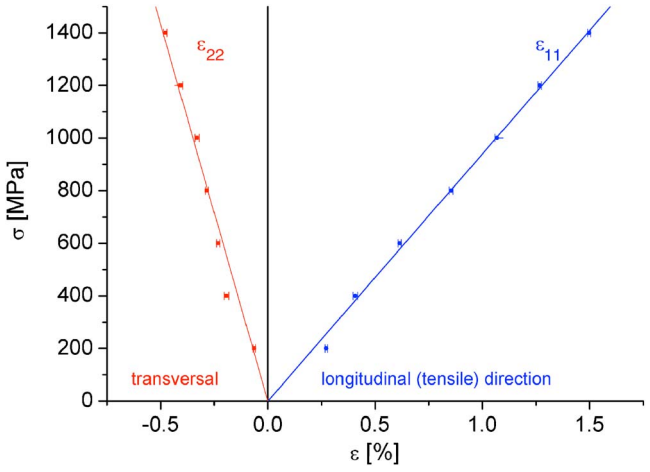

FIG. 5. (Color online) Stress-strain curves for different strain tensor components. The lines correspond to the fit of the data to a linear function starting from the origin of the coordinate system.

With increasing tensile load it becomes elliptical. The changes are most pronounced for the first and strongest diffuse ring appearing in the 2D XRD pattern. To describe such changes more quantitatively one has to construct the set of symmetrized intensity distributions according to Eq. (1) and trace the change in the first peak position as a function of azimuth angle, φ, and tensile stress, σ. It should be noted here that no changes were observed between seven diffraction patterns, independently acquired along the length of the sample (1 mm steps), when holding the load at a fixed value of external stress. The experimental scatter of the measured strain values at each different stress levels for seven independent locations along the gauge length is shown as error bars in Figs. 3 and 4. From Fig. 3 it is evident that the asymmetry of the first diffuse maximum increases with increasing load. The decrease in the peak position with increasing tensile stress (the curve corresponding to φ=90° or the blue curve in Fig. 3) reflects the fact that atoms move apart along the tensile direction. An opposite behavior is seen in transversal direction (the curve corresponding to φ=0° or the red curve in Fig. 3).

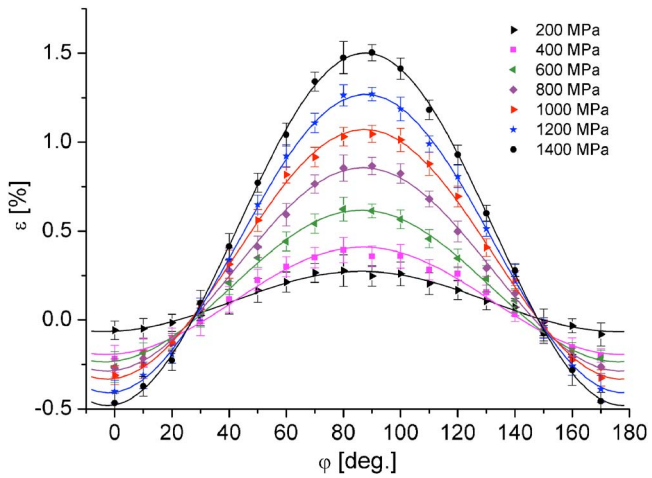

FIG. 4. (Color online) Angular dependence of the strain determined at various stages of tensile deformation. The full lines denote fits of the experimental data to Eq. (4).

Figure 4 shows the angular variation of the strain ε at a given stress σ as calculated from the relative change in the position of the first peak using Eq. (3). The fit of the experimental data to Eq. (4) yields two components of the strain tensor, ε_{11} and ε_{22} (the axial and tangential components, respectively). The stress-strain curves as observed for different strain tensor components are plotted in Fig. 5. Within the experimental error all of them show a linear behavior thus indicating the elastic regime of the tensile deformation for the investigated specimens. The samples fractured at a stress of about 1500 MPa and did not provide any hint for yielding, despite the fact that the compressive yield strength of this BMG was reported to be 1690–1851 MPa.[28] This different behavior indicates a significant strength asymmetry for this BMG.[41] The maximum axial strain (ε_{11}) achieved is $1.50 \pm 0.01\%$. The elastic modulus determined in tensile mode is $E_{11}=94 \pm 1$ GPa, and the experimentally determined Poisson's ratio $n(=-\varepsilon_{22}/\varepsilon_{11}=-E_{11}/E_{22})$ is 0.325 ± 0.01.

B. Evolution of local atomic structure upon tensile deformation

Figure 6 shows the structure factor of the $Zr_{64.13}Cu_{15.75}Ni_{10.12}Al_{10}$ BMG at different stages of deformation. It should be noted that the structure factors shown in Fig. 6 were calculated using Eq. (5) from the corresponding symmetrized intensity distributions, derived along the tensile direction (φ=90°). From the inset in Fig. 6 it is evident that the position of the first maximum shifts toward lower Q values with increasing tensile stress. In order to relate these changes in reciprocal space with real space one has to perform a Fourier transformation of the structure factor $S(Q)$ according Eq. (6). Figure 7 shows the pair distribution functions $g(r)$ calculated from the corresponding $S(Q)$ data by applying Eqs. (6) and (7). The inset in Fig. 7 gives a detailed view of the first broad maximum appearing in $g(r)$ together with the interatomic bond lengths[42] and the corresponding weight factors w_{ij} calculated at Q=0 Å^{-1} (denoted by filled circles and explicitly listed in Table I).

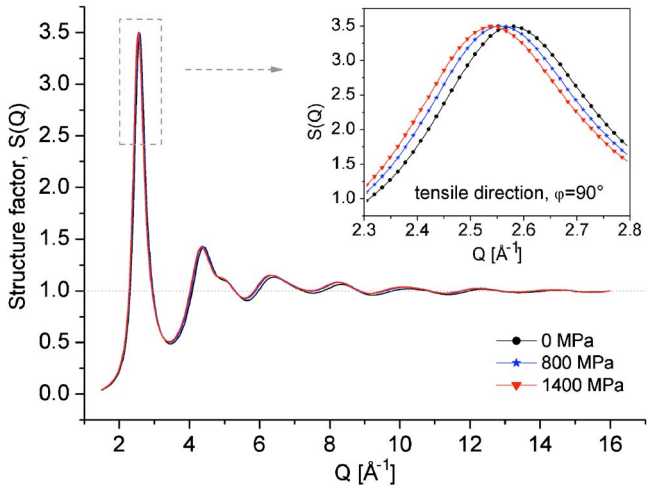

FIG. 6. (Color online) Total structure factor $S(Q)$ of $Zr_{64.13}Cu_{15.75}Ni_{10.12}Al_{10}$ metallic glass at different stages of deformation. The inset shows how the position of the first peak changes with applied tensile stress when observed in tensile direction (φ=90°).

From the type and concentration of the constituent elements in the $Zr_{64.13}Cu_{15.75}Ni_{10.12}Al_{10}$ alloy, it is clear that Zr–Zr, Zr–Cu, and Zr–Ni are the dominant atomic pairs which constitute the first coordination shell of the PDFs. In view of Table I, one can find that the weight averages w_{ij} of the remaining partials are negligibly small due to low concentrations of Cu, Ni, and Al as well as their relatively weak scattering powers. Since Cu and Ni are almost identical with respect to their atomic radii,[42] only two partials [Zr–(Cu,Ni) and Zr–Zr] need to be resolved. Figure 8(a) shows the result of the deconvolution for the first shell of undeformed $Zr_{64.13}Cu_{15.75}Ni_{10.12}Al_{10}$. The center of the first peak was estimated to be at 2.68 Å (red curve) corresponding to Zr–(Cu,Ni) atomic pairs. The major component centered at 3.14 Å (blue curve) originates from Zr–Zr atomic pairs. As can be seen from Fig. 8(b), an increase in tensile stress shifts both peaks toward higher r values (see Table II). This implies that tensile stress increases the average atomic distances along the loading direction.

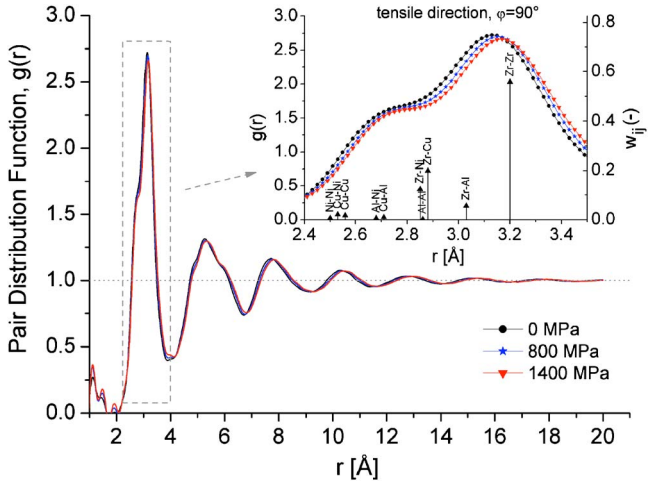

FIG. 7. (Color online) PDFs $g(r)$ of $Zr_{64.13}Cu_{15.75}Ni_{10.12}Al_{10}$ metallic glass at different stages of deformation. The inset shows a zoomed view of the first coordination shell. The dots refer to the interatomic bond lengths calculated as a sum of the atomic (metallic) radii (listed in Table I).

TABLE I. Ten possible nearest-neighbor atomic pairs in $Zr_{64.13}Cu_{15.75}Ni_{10.12}Al_{10}$ metallic glass and their theoretical bond lengths [R_{ij}^0, the sum of atomic radii (1.6, 1.28, 1.43, and 1.25 Å for Zr, Cu, Al, and Ni, respectively)] and weighting factors w_{ij} calculated at Q=0 Å^{-1} according to Eq. (11).

i-j	R_{ij}^0 (Å)	w_{ij}
Zr–Zr	3.20	0.557
Zr–Cu	2.88	0.199
Zr–Ni	2.85	0.123
Zr–Al	3.03	0.057
Cu–Cu	2.56	0.018
Cu–Al	2.71	0.010
Cu–Ni	2.53	0.022
Al–Al	2.86	0.001
Al–Ni	2.68	0.006
Ni–Ni	2.50	0.007

IV. DISCUSSION

Despite the excellent plasticity observed under compressive loading,[28] the $Zr_{64.13}Cu_{15.75}Ni_{10.12}Al_{10}$ BMG fractured without showing any hint of macroplasticity in the current

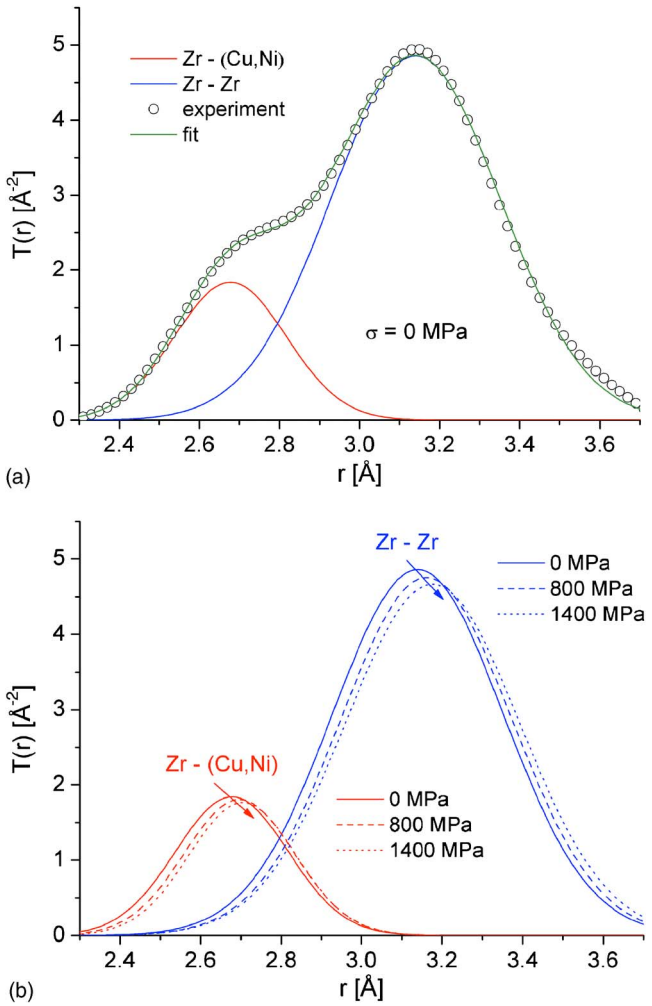

FIG. 8. (Color online) (a) Deconvolution of the first coordination shell into two Gaussians for an unloaded sample and (b) at different stages of deformation.

TABLE II. Best-fit peak position r_{ij} (± 0.01 Å) obtained from decomposition of the first coordination shell. The last column contains the average coordination number N (± 0.2), calculated from the RDF(r) in the interval 2–3.85 Å.

σ (MPa)	$r_{Zr-(Cu,Ni)}$ (Å)	r_{Zr-Zr} (Å)	N
0	2.68	3.14	13.4
800	2.70	3.16	13.5
400	2.71	3.18	13.6

tensile tests. The linear shift of the peak position with applied load (Fig. 3), and the perfect linear dependence of the stress with increasing strain (Fig. 5) indicate a purely elastic behavior in the overall structure. The Young modulus (E) and Poisson's ratio (ν) calculated from the strain tensor are 94 GPa and 0.325, respectively. The elastic constants, measured previously[28] by ultrasonic methods revealed different values: 78.41 GPa for E and 0.377 for ν. The different values for the elastic modulus can be easily explained if one assumes that the stiffness of the first, second, third, and consecutive atomic shells is different. The diffraction measurements may detect such differences, while ultrasound techniques average the elastic constants of different shells and measure the bulk properties of the material. Such differences were recently reported also by other authors and the available data are summarized in Table III.

Das *et al.*[34] recently investigated two different BMGs, one brittle ($Zr_{55}Cu_{20}Ni_{10}Al_{10}Ti_5$) and one ductile ($Cu_{47.5}Zr_{47.5}Al_5$), by *in situ* compression testing under synchrotron radiation: these investigations also revealed differences between the values of the elastic constants obtained from x-ray and ultrasonic sound velocity measurements. In this case, Young's modulus derived from the strain tensors took values higher than those measured by ultrasound methods, but the values of Poisson's ratio were very close, i.e., almost the same. It is interesting to follow the differences in the values presented by different authors (see Table III): for brittle BMG ($Zr_{55}Cu_{20}Ni_{10}Al_{10}Ti_5$),[34] the difference in Young's modulus is less than 6 GPa (85.5 GPa from ultrasound measurements compared to 91.1 GPa from the strain tensor) and Poisson's ratio is virtually the same (0.378 from ultrasound and 0.38 from the strain tensor), while for ductile BMG ($Cu_{47.5}Zr_{47.5}Al_5$) (Ref. 34) the differences are larger: 90.1 GPa (from ultrasound measurements) compared to 99.2 GPa (strain tensor) for Young's modulus and 0.365 (ultrasound measurements) or 0.34 (strain tensor calculations) in the case of Poisson's ratio. Other work which deals with the strain tensor measured upon XRD and was reported by Wang *et al.*[35] They also noticed such differences in the case of $Zr_{62}Al_8Ni_{13}Cu_{17}$ and $La_{62}Al_{14}(Cu_{5/6}Ag_{1/6})_{14}Co_5Ni_5$ BMGs. In our present study, these differences follow the same trend but they are even larger, i.e., 16 GPa for Young's modulus and 0.052 for Poisson's ratio. In the same time, it was shown that the studied $Zr_{64.13}Cu_{15.75}Ni_{10.12}Al_{10}$ BMG shows a much larger compressive strain (160%) (Ref. 28) than the previously investigated $Cu_{47.5}Zr_{47.5}Al_5$ BMG (0.7% plastic deformation).[34] Judging from the trend of the values of the elastic constants summarized in Table III, as measured by ultrasonic methods and as calculated from the strain tensor measured by diffraction experiments, it is very clear that in the case of "nondeformable" or intrinsically brittle BMGs, the bulk elastic constants as derived from ultrasound measurements and the ones obtained from the strain tensor analysis are almost similar, indicating a similar elastic behavior of each atomic shell. In the case of plastically deformable BMGs each atomic shell has a different stiffness, as revealed from the large differences of the elastic constants from ultrasonic and tensor analysis. Most likely, such local fluctuations of the elastic properties in the glassy structure can rather easily induce local shear transformation[44] and, thus, the BMG exhibits macroscopic plasticity. However, more experimental work is needed to clarify the atomic-scale origin of the macroscopic plasticity in metallic glasses.

TABLE III. Reported Young's modulus (E) and Poisson's ratio (ν) values for different BMGs. "USV" denotes the values measured by ultrasonic methods and "x-ray" those measured by means of the strain tensor deduced from *in situ* XRD using synchrotron radiation.

Composition	E_{usv} (GPa)	υ_{usv}	$E_{x\text{-}ray}$ (GPa)	$n_{x\text{-}ray}$
$Zr_{64.13}Cu_{15.75}Ni_{10.12}Al_{10}$ [a]	78	0.377	94	0.325
$Cu_{47.5}Zr_{47.5}Al_5$ [b]	90.1	0.365	99.2	0.34
$Zr_{55}Cu_{20}Ni_{10}Al_{10}Ti_5$ [b]	85.5	0.378	91.1	0.38
$Zr_{62}Al_8Ni_{13}Cu_{17}$ [c]	80	0.38	83	0.37
$La_{62}Al_{14}(Cu_{5/6}Ag_{1/6})_{14}Co_5Ni_5$ [c]	35	0.36	34	0.36
$Mg_{60}Cu_{30}Y_{10}$	51.5 ± 1.5 [d]	n.a.	64.1[e]	0.373[e]

[a]Present work.
[b]Reference 34.
[c]Reference 35.
[d]Reference 43.
[e]Reference 29.

V. CONCLUSIONS

In the past years a universal diffraction method for characterizing bulk stress and strain fields in amorphous materials was established. This method, employing synchrotron radiation, was applied in this work in order to study the *in situ* behavior of $Zr_{64.13}Cu_{15.75}Ni_{10.12}Al_{10}$ BMG at different stages of tensile deformation. Despite a large compressive deformability previously reported, the $Zr_{64.13}Cu_{15.75}Ni_{10.12}Al_{10}$ BMG fractured without showing any hint of macroplasticity in the current tensile tests. The linear shift of the peak position with applied load and the perfect linear dependence of the stress with increasing strain indicate a purely elastic behavior in the overall structure. The elastic constants calculated from the strain tensor are different from those measured by ultrasonic techniques. These differences are supposed to arise because the ultrasound techniques average the elastic constants of different atomic shells and measure the bulk properties of the material, while the diffraction measurements may detect differences in stiffness of the first, second, third, and consecutive atomic shells.

The position of the first diffraction broad maximum shifts toward lower Q values with increasing tensile stress. In the real space, this implies that tensile stress increases the average atomic distances along the loading direction. Due by

the type and concentration of the constituent elements in the $Zr_{64.13}Cu_{15.75}Ni_{10.12}Al_{10}$ alloy, it is concluded that Zr–Zr, Zr–Cu, and Zr–Ni are the dominant atomic pairs which constitute the first coordination shell of the PDFs.

ACKNOWLEDGMENTS

The financial support of the EU through the European Research and Training Network "Ductile BMG Composites" (Contract No. MRTN-CT-2003-504692) was fully acknowledged. The authors thank S. Venkataraman, S. Pauly, and U. Siegel for helpful discussions and W. Lösel for sample preparation.

[1]W. L. Johnson, MRS Bull. **24**, 42 (1999).
[2]A. Inoue, Acta Mater. **48**, 279 (2000).
[3]C. A. Pampillo, J. Mater. Sci. **10**, 1194 (1975).
[4]F. Spaepen, Acta Metall. **25**, 407 (1977).
[5]A. S. Argon, Acta Metall. **27**, 47 (1979).
[6]P. S. Steif, F. Spaepen, and J. W. Hutchinson, Acta Metall. **30**, 447 (1982).
[7]P. E. Donovan, Acta Mater. **37**, 445 (1989).
[8]H. Chen, Y. He, G. J. Shiflet, and S. J. Poon, Nature (London) **367**, 541 (1994).
[9]S. Venkataraman, M. Stoica, S. Scudino, T. Gemming, C. Mickel, U. Kunz, K. B. Kim, L. Schultz, and J. Eckert, Scr. Mater. **54**, 835 (2006).
[10]M. Stoica, J. Eckert, S. Roth, Z. F. Zhang, L. Schultz, and W. H. Wang, Intermetallics **13**, 764 (2005).
[11]U. Kühn, J. Eckert, N. Mattern, and L. Schultz, Appl. Phys. Lett. **77**, 3176 (2000).
[12]J. Eckert, Mater. Sci. Eng., A **226–228**, 364 (1997).
[13]R. Busch, E. Bakke, and W. L. Johnson, Acta Mater. **46**, 4725 (1998).
[14]S. C. Glade and W. L. Johnson, J. Appl. Phys. **87**, 7249 (2000).
[15]C. T. Liu, L. Heatherly, J. A. Horton, D. S. Easton, C. A. Carmichael, J. L. Wright, J. H. Schneibel, M. H. Yoo, C. H. Chen, and A. Inoue, Metall. Mater. Trans. A **29**, 1811 (1998).
[16]G. He, J. Lu, Z. Bian, D. J. Chen, G. L. Chen, G. C. Tu, and G. J. Chen, Mater. Trans. **42**, 356 (2001).
[17]A. Inoue, H. M. Kimura, and T. Zhang, Mater. Sci. Eng., A **294–296**, 727 (2000).
[18]Z. F. Zhang, G. He, J. Eckert, and L. Schultz, Phys. Rev. Lett. **91**, 045505 (2003).
[19]Z. F. Zhang, J. Eckert, and L. Schultz, Acta Mater. **51**, 1167 (2003).
[20]A. L. Greer, Science **267**, 1947 (1995).
[21]L. Q. Xing, Y. Li, K. T. Ramesh, J. Li, and T. C. Hufnagel, Phys. Rev. B **64**, 180201 (2001).
[22]J. J. Lewandowski and A. L. Greer, Nat. Mater. **5**, 15 (2006).
[23]D. M. Dimiduk, C. Woodward, R. LeSar, and M. D. Uchic, Science **312**, 1188 (2006).
[24]J. Das, M. B. Tang, K. B. Kim, R. Theissmann, F. Baier, W. H. Wang, and J. Eckert, Phys. Rev. Lett. **94**, 205501 (2005).
[25]Z. F. Zhang, H. Zhang, X. F. Pan, J. Das, and J. Eckert, Philos. Mag. Lett. **85**, 513 (2005).
[26]H. Bei, S. Xie, and E. P. George, Phys. Rev. Lett. **96**, 105503 (2006).
[27]J. Schroers and W. L. Johnson, Phys. Rev. Lett. **93**, 255506 (2004).
[28]Y. H. Liu, G. Wang, R. J. Wang, D. Q. Zhao, M. X. Pan, and W. H. Wang, Science **315**, 1385 (2007).
[29]H. F. Poulsen, J. A. Wert, J. Neuefeind, V. Honkimäki, and M. Daymond, Nat. Mater. **4**, 33 (2005).
[30]H. W. Sheng, H. Z. Liu, Y. Q. Cheng, J. Wen, P. L. Lee, W. K. Luo, S. D. Shastri, and E. Ma, Nat. Mater. **6**, 192 (2007).
[31]A. R. Yavari, A. Le Moulec, A. Inoue, N. Nishiyama, N. Lupu, E. Matsubara, W. J. Botta, G. Vaughan, M. Di Michiel, and Å. Kvick, Acta Mater. **53**, 1611 (2005).
[32]R. T. Ott, F. Sansoz, J. F. Molinari, J. Almer, K. T. Ramesh, and T. C. Hufnagel, Acta Mater. **53**, 1883 (2005).
[33]D. K. Balch, E. Ustundag, and D. C. Dunand, Metall. Mater. Trans. A **34**, 1787 (2003).
[34]J. Das, M. Bostrom, N. Mattern, A. Kvick, A. R. Yavari, A. L. Greer, and J. Eckert, Phys. Rev. B **76**, 092203 (2007).
[35]X. D. Wang, J. Bednarcik, K. Saksl, H. Franz, Q. P. Cao, and J. Z. Jiang, Appl. Phys. Lett. **91**, 081913 (2007).
[36]H. F. Poulsen, J. Neuefeind, H. B. Neumann, J. R. Schneider, and M. D. Zeidler, J. Non-Cryst. Solids **188**, 63 (1995).
[37]A. P. Hammersley, S. O. Svensson, M. Hanfland, A. N. Fitch, and D. Häusetmann, High Press. Res. **14**, 235 (1996).
[38]T. Egami and S. J. L. Billinge, *Underneath the Bragg Peaks: Structural Analysis of Complex Materials* (Pergamon, New York/Elsevier, Oxford, England, 2003).
[39]I. K. Jeong, J. Thompson, Th. Proffen, A. Perez, and S. J. L. Billinge, J. Appl. Crystallogr. **34**, 536 (2001).
[40]D. A. Dimitrov, H. Roder, and A. R. Bishop, Phys. Rev. B **64**, 014303 (2001).
[41]C. A. Schuh and A. C. Lund, Nat. Mater. **2**, 449 (2003).
[42]*ASM Handbook: Metals Handbook* (ASM International, Materials Park, OH, 1992), Vols. 1 and 2.
[43]A. Castellero, S. J. Lloyd, S. V. Madge, Zs. Kovacs, J. F. Löffler, M. Baricco, and A. L. Greer, J. Alloys Compd. **434–435**, 48 (2007).
[44]M. L. Falk, J. S. Langer, and L. Pechenik, Phys. Rev. E **70**, 011507 (2004).